Petroleum Science 21 (2024) 1032–1043

Contents lists available at ScienceDirect

Petroleum Science

journal homepage: www.keaipublishing.com/en/journals/petroleum-science

Original Paper

Phase behavior of gas condensate in porous media using real-time computed tomography scanning

Wen-Long Jing [a, b], Lei Zhang [a, b, *], Ai-Fen Li [a, b], Jun-Jie Zhong [a, b], Hai Sun [a, b], Yong-Fei Yang [a, b], Yu-Long Cheng [a, b], Jun Yao [a, b]

[a] Institute of Petroleum Engineering, China University of Petroleum (East China), Qingdao, 266580, Shandong, China
[b] National Key Laboratory of Deep Oil and Gas, China University of Petroleum (East China), Qingdao, 266580, Shandong, China

ARTICLE INFO

Article history:
Received 14 May 2023
Received in revised form
6 November 2023
Accepted 8 November 2023
Available online 11 November 2023

Edited by Yan-Hua Sun

Keywords:
Gas condensate
Pressure depletion
Real-time micro-computed tomography scanning
Distribution of condensate liquid

ABSTRACT

The phase behavior of gas condensate in reservoir formations differs from that in pressure–volume–temperature (PVT) cells because it is influenced by porous media in the reservoir formations. Sandstone was used as a sample to investigate the influence of porous media on the phase behavior of the gas condensate. The pore structure was first analyzed using computed tomography (CT) scanning, digital core technology, and a pore network model. The sandstone core sample was then saturated with gas condensate for the pressure depletion experiment. After each pressure-depletion state was stable, real-time CT scanning was performed on the sample. The scanning results of the sample were reconstructed into three-dimensional grayscale images, and the gas condensate and condensate liquid were segmented based on gray value discrepancy to dynamically characterize the phase behavior of the gas condensate in porous media. Pore network models of the condensate liquid ganglia under different pressures were built to calculate the characteristic parameters, including the average radius, coordination number, and tortuosity, and to analyze the changing mechanism caused by the phase behavior change of the gas condensate. Four types of condensate liquid (clustered, branched, membranous, and droplet ganglia) were then classified by shape factor and Euler number to investigate their morphological changes dynamically and elaborately. The results show that the dew point pressure of the gas condensate in porous media is 12.7 MPa, which is 0.7 MPa higher than 12.0 MPa in PVT cells. The average radius, volume, and coordination number of the condensate liquid ganglia increased when the system pressure was between the dew point pressure (12.7 MPa) and the pressure for the maximum liquid dropout, P_{max} (10.0 MPa), and decreased when it was below P_{max}. The volume proportion of clustered ganglia was the highest, followed by branched, membranous, and droplet ganglia. This study provides crucial experimental evidence for the phase behavior changing process of gas condensate in porous media during the depletion production of gas condensate reservoirs.

1. Introduction

A gas condensate reservoir is a special gas reservoir whose formation temperature is between the critical temperature and the temperature for maximum liquid dropout under the original formation conditions (Zhang et al., 2020; Raghavan and Jones, 1996; Tu et al., 2022). A high gas–oil ratio (GOR) and high content of light components are the main characteristics of gas condensate reservoirs (Noor et al., 2020; Reis and Carvalho, 2022; Faraji et al., 2019). The hydrocarbon mixture in the gas condensate reservoir exists in the gas phase at the original temperature and pressure of formation. Unlike conventional reservoirs, in which oil or gas usually maintains a single phase above the bubble point pressure (Zhu et al., 2020), the formation pressure keeps changing during the development of gas condensate reservoirs, resulting in continuous changes in the phase behavior of the gas condensate in the formation (Wang et al., 2022; Li et al., 2017b). Condensate liquid and gas condensate both appear in porous media during their development (Luo et al., 2021). This phenomenon can cause certain

* Corresponding author. Institute of Petroleum Engineering, China University of Petroleum (East China), Qingdao, 266580, Shandong, China.
E-mail address: zhlei84@163.com (L. Zhang).

https://doi.org/10.1016/j.petsci.2023.11.009

difficulties in the development of gas condensate reservoirs because, in the process of depletion production, if the phase behavior of the gas condensate changes, the condensate liquid will remain in the formation, resulting in a reduction in the gas condensate reservoir recovery (Will et al., 2018). Therefore, for gas condensate reservoir development, it is important to study the phase behavior of the gas condensate in a formation with constantly changing pressure.

The traditional method for investigating the phase behavior of gas condensate is to determine the relationship between the pressure, temperature, and volume (PVT) of the gas condensate through experimental methods (Dodson et al., 1953). The phase behavior experiment of a gas condensate is the same as that of a fluid in conventional reservoirs in principle (Moses, 1986), but there are differences in the experimental equipment and methods. Currently, gas condensate phase behavior experiment is commonly conducted in PVT cells with observation windows (WcCain, 2002). Constant volume depletion (CVD) and constant component expansion (CCE) are the most commonly used experiments in PVT cells to simulate the phase behavior changing process of gas condensate during the development of gas condensate reservoirs (Potsch et al., 2017). Although these experiments can provide important high-pressure physical parameters of gas condensate, they have limitations that cannot be ignored. It is well known that gas condensate exists in the porous media of formations, and that the phase behavior of the gas condensate is different in porous media and PVT cells (Guo et al., 1996; Saeidi and Handy, 1974; Shapiro et al., 2000). The adsorption and capillary condensation caused by pores and throats in porous media on condensate gas can affect their physical properties (Nguyen et al., 2015; Zhong et al., 2018a). The interior of the PVT cells is a cavity, which cannot represent the complex structure of porous media in actual formations. Therefore, the characteristic parameters of the gas condensate obtained from conventional PVT experiments are not accurate.

In some early studies, to simulate real conditions in the production of gas condensate depletion production in laboratory experiments, quartz sand, glass beads, and steel beads were filled into PVT cells as a porous medium (Weinaug and Cordell, 1949; Sigmund et al., 1973). A methane-*n*-pentane binary gas condensate was used to conduct pressure depletion production experiments to study the effect of porous media on the phase behavior of the gas condensate. The dew point pressure and volume fraction of the condensate liquid were recorded, and the composition of the gas discharged under different pressures was analyzed using gas chromatography. After comparing the results from different models, it was found that the dew point pressure of the gas condensate system under different filling media conditions was the same (Shapiro and Stenby, 1999). Therefore, it was concluded that the porous media had no influence on the phase behavior of the gas condensate. However, the equipment used in these experiments was underdeveloped in the past times when these studies were conducted. In addition, the fillers used in the models were significantly different from those used in real porous media. Furthermore, the components of the gas condensate were too simple for a realistic representation.

With the development of electronic computers and programming technology, artificial intelligence has been widely applied in multiple fields. The measurements of phase characteristics of gas condensate are cumbersome and time-consuming, in order to improve efficiency, artificial intelligence has been used to figure out the problems. An intelligent approach based on least square support vector machine (LSSVM) modeling was developed for prediction of dew-point pressure in gas condensate reservoirs (Arabloo et al., 2013). The model was developed based on 562 experimental results from different gas condensate reservoirs all over the world. The predicted results are basically consistent with the experimental results and the variation of dew point pressure with temperature can be simulated by the model. In addition, models established based on CVD, chemical composition, reserve temperatures, and fluid characteristics also play an important role in predicting the dew point pressure of gas condensate (Ghiasi et al., 2014; Gouda et al., 2022). These models were based on big data from 453 to 1300 gas condensate samples worldwide, and the average absolute relative deviation and correlation coefficient of the developed models are 0.73%–5.03% and 0.953–0.998, respectively. However, the predictions based on artificial intelligence can depend heavily on the roughness of the data set and the size of data samples. Although experimental operations are avoided, obtaining big data is also challenging. Besides, this method, like the traditional PVT experiment, cannot consider the influence of porous media on the phase behavior of gas condensate.

In recent years, some investigations have improved the experimental methods to study the influence of porous media on the phase behavior of gas condensate (Li et al., 2013; Sui et al., 2010; Tong et al., 2004). Long cores were used as the research objects in the gas condensate pressure depletion experiments. The gas condensate was compounded by methane-*n*-pentane. After comparing the results of the CVD experiment conducted in the PVT cells, it was found that the large specific surface area caused the porous media to absorb heavy hydrocarbon components under high pressure, resulting in a significant increase in the dew point pressure of the gas condensate in cores (Qi et al., 2007). Although these studies have proven that porous media can affect the phase behavior of gas condensate, many problems remain. First, the composition of the gas condensate used in these studies was too simple to reflect the characteristics of gas condensate with complex compositions in their actual reservoirs. In addition, the dynamic phase behavior changing process of the gas condensate in porous media cannot be reflected. Thus, studying the influence mechanism of porous media on the phase behavior of gas condensate needs further improvement.

In this study, a sandstone was used as the research object to investigate the dynamic evolution of the phase behavior of multicomponent gas condensate in porous media. The gas condensate was compounded based on its components in an actual gas condensate reservoir. First, the pore structure of the sandstone was analyzed. Then, a gas condensate pressure depletion experiment was conducted in the sandstone using real-time CT scanning to obtain the distribution of the gas condensate and condensate liquid under different pressures. Pore network models were built to calculate and analyze the typical structural parameters of condensate liquid ganglia. Finally, four types of condensate liquid were classified by the shape factor and Euler number to describe the morphological changing process of condensate liquids dynamically and elaborately in porous media.

2. Materials and experimental methods

2.1. Sample and fluid preparation

An artificial sandstone with a diameter of 2.5 cm and a length of 6.2 cm was prepared in a core barrel by mixing quartz sand (4×10^7 μm^3) with oil-based epoxy resin at a mass ratio of quartz sand to oil-based epoxy resin of 25:1 and used as the research object in this study. The resolution of the CT scanning images is related to the distance of the X-ray source and the detector from the sample (Wu et al., 2022; Hemes et al., 2015; Li Y. et al., 2022). The closer the X-ray source and detector are to the sample, the higher the resolution of the scanned images and the clearer the images (Sun et al., 2018; Masihi et al., 2022; Fang et al., 2023). Therefore, to

ensure that the CT scanning results accurately reflect the pore and throat distribution, the sandstone was cut into a small sample with a diameter of 5 mm and a length of 8 mm. The sample-to-detector and source-to-sample distances were 25 and 35 mm, respectively. The resolution of the CT scanning images was 3.977 μm.

The components of the gas condensate used in this study are listed in Table 1. The flash gas–oil ratio (GOR) of the gas condensate is 15,813 g/m^3. The classification of hydrocarbon fluids can be based on the composition analysis of the fluid mixture, which has one of the strongest effects on the fluid characteristics, as shown in the ternary diagram (Ahmed, 2016; Mansour et al., 2020), and presented in Fig. 1. The composition of the gas sample used in the experiment is in the area of the gas condensate system, proving that the gas sample used is gas condensate. The pressure–temperature (P–T) diagram of the gas condensate sample is shown in Fig. 2. The gas condensate was prepared using different gas and liquid hydrocarbon samples with a purity of 99.999%. After calculating the volume of each hydrocarbon component based on the gas state equation (Li and Yu, 2022), we first accurately weighed liquid hydrocarbons with a measuring cylinder and added them to the FY-III sample preparation apparatus. Then we transferred the gas into the FY-III sample preparation apparatus in order of saturation pressure of each gas component from low to high. After that, we increased the pressure and temperature of the FY-III sample preparation apparatus to 16.0 MPa and 70 °C, and the apparatus automatically shook to mix the fluid evenly for 4 h to form a single-phase fluid. Finally, we maintained the pressure unchanged, slowly opened the outlet valve, and used a gas collection bag to slowly collect a small amount of fluid samples for gas chromatograph detection. If the difference between the content of each component in the prepared gas condensate and the actual content in Table 1 is less than 3%, it is considered qualified for sample preparation.

The gas condensate was then subjected to CCE tests in a PVT cell, as shown in Fig. 3. The middle of the image shows a piston with gas condensate above the piston and water below it. As the pressure decreased, the piston continuously moved downwards. At 14.0 and 13.0 MPa, the gas condensate above the piston had good transparency and remained a single gas phase. When the pressure was 12.0 MPa, the transparency of the area above the piston decreased. At this pressure, the condensate gas reached the dew point and began to undergo a phase transition from the gaseous state to a foggy state. When the pressure decreased from 11.0 to 5.0 MPa, the condensate liquid precipitated, and the liquid volume first increased and then decreased. The CCE test result shows that the dew point pressure and the pressure for the maximum liquid dropout of gas condensate in the PVT cell are 12.0 MPa and 9.0 MPa, respectively, at 70 °C.

Table 1
Gas condensate composition.

Component	Molar composition of gas condensate, %
CO_2	7.90
N_2	0.60
C_1	70.82
C_2	11.80
C_3	4.19
n-C_4	2.11
n-C_5	0.85
C_6	0.67
C_7	0.45
C_8	0.14
C_9	0.18
C_{10}	0.29
Total	100.00

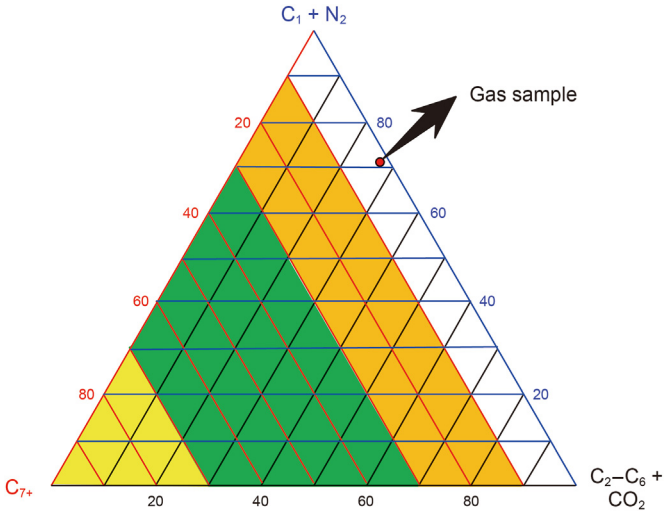

Fig. 1. Compositions of different types of reservoir fluids. The *yellow* area represents gas condensate system, the *green* area represents volatile oil system, the *orange* area represents ordinary black oil system and the *white* area represents low shrinkage oil system.

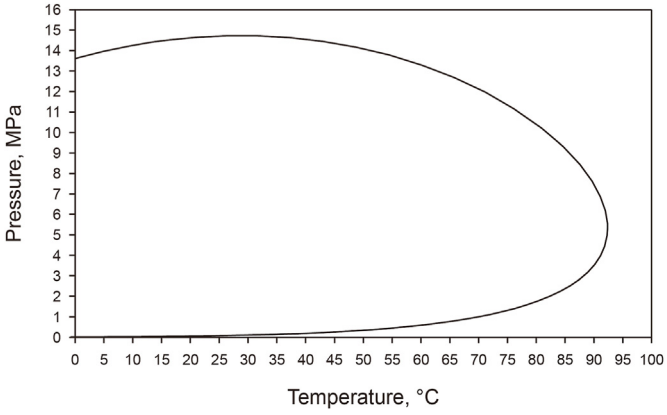

Fig. 2. Pressure–temperature phase diagram of gas condensate.

2.2. Experimental setup and procedure

The temperature was set to 70 °C for the experiment. The instruments included a core holder, a high-pressure temperature-controlled intermediate container, pressure gauges, ISCO pumps with a velocity accuracy of 0.0001 cm^3/min, an incubator, a vacuum pump, and a micro-CT scanner. The experimental procedure and devices used are presented in Fig. 4. First, all experimental devices were vacuumed. CT scanning of the dry core sample was performed to obtain the initial pore structure. Then, the gas condensate was injected into the core sample at a constant pressure (4.0 MPa higher than the dew point pressure of the gas condensate under the same conditions in the PVT cell) from the intermediate container to maintain a single-phase gas state. The core sample was saturated with gas condensate. After the system stabilized for 4 h, the sample was scanned using CT to obtain images of the saturated gas condensate in the pores and throats. The gas condensate system was depressurized with a depressurization gradient of 1.0 MPa. After the system was stable for 0.5 h, the sample was scanned again to observe the phase behavior of the gas condensate in the CT scanning images. When obvious gray value changes were observed in the CT scanning images of the pores, the condensate liquid had

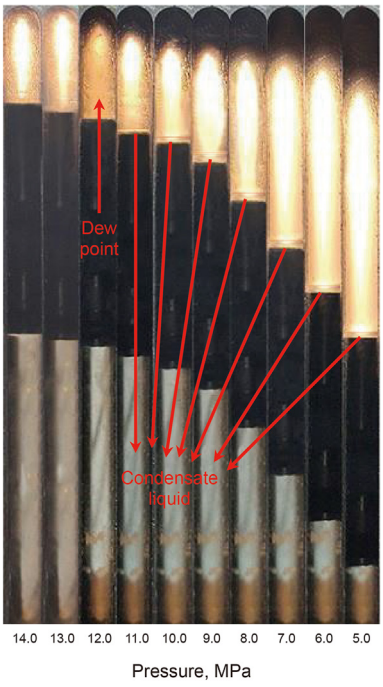

Fig. 3. Image of gas condensate and condensate liquid in PVT cylinders under different pressures.

appeared (Li M. et al., 2022; Hong et al., 2023). To accurately determine the dew point pressure of the gas condensate in the sandstone, the pressure was increased by 1.0 MPa, and after the system stabilized, the pressure was reduced at a depressurization gradient of 0.1 MPa. CT scanning was performed after each depressurization and system stabilization to obtain an accurate dew point pressure of the gas condensate in the sandstone. Subsequently, the system was continually depressurized with 1.0 MPa as the depressurization gradient, and CT scanning was performed at each pressure. It is noted that to exclude the faults of the statistics and the experimental errors, the measurement was repeated at least three times, and the error of each measurement result was ensured to not exceed 1%. The following study presents the results and analysis of one set of the measurements.

3. Results and discussion

3.1. Pore structure analysis

A representative elementary volume (REV) with a voxel size of 400 × 400 × 400 was extracted from the sandstone CT scanning data. However, due to external interference in the scanning process, the obtained images have problems such as being dark or bright, low contrast, and having a lot of noise in the image. Therefore, it is necessary to perform brightness, contrast, and filtering processing on the images to improve their quality (Buades et al., 2005). Afterwards, the pores and skeletons of the sandstone were extracted separately to establish a 3D digital core. We used the watershed algorithm for segmentation of the images (Saarinen, 1994; Meyer, 1994). The watershed algorithm is a segmentation algorithm based on morphology and topography, which is a gradient segmentation of images (Scanziani et al., 2018; Cousty et al., 2009). Due to the strong grayscale changes at the phase edges, gradient images

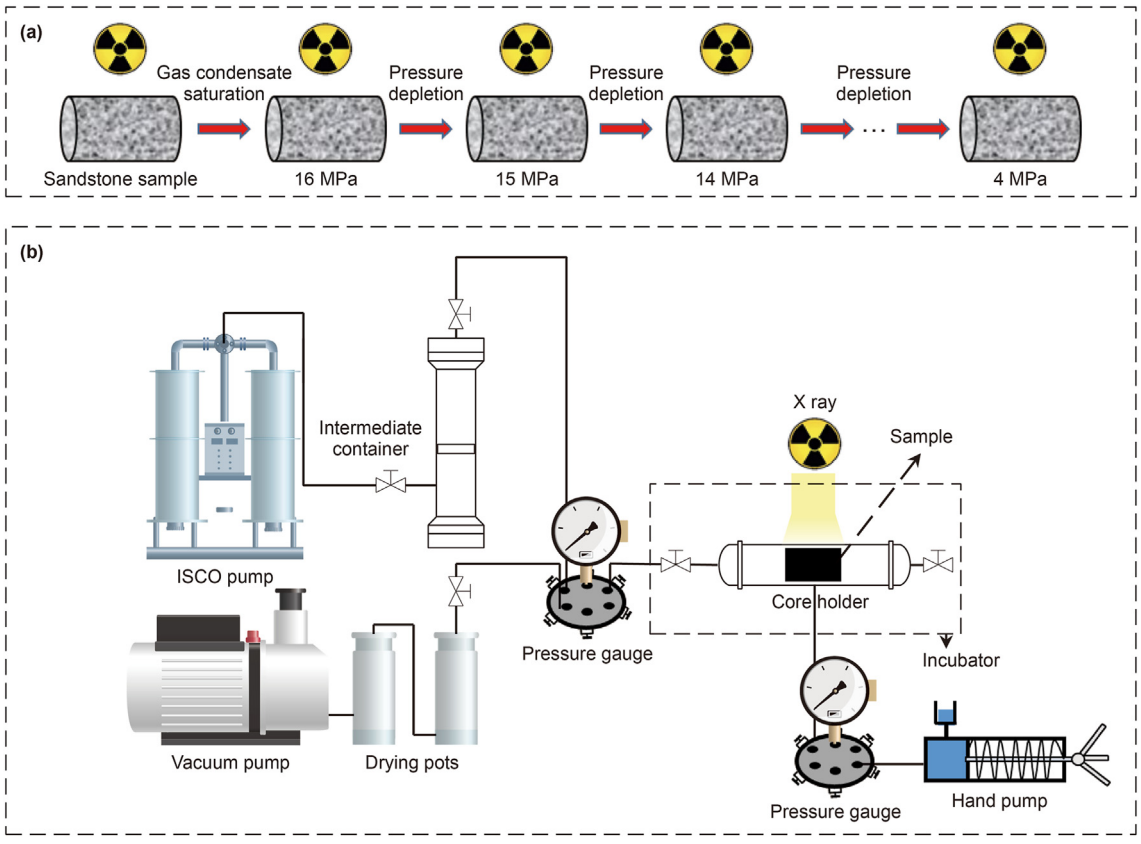

Fig. 4. Sequence of experimental procedures (**a**) and the schematic diagram of experimental setup (**b**).

precisely describe the grayscale changes of the images (Barnes et al., 2014). Therefore, the original images can be first divided into grayscale gradient images through gradient partitioning, and then segmentation can be performed through watershed transformation of the gradient image. The 3D digital core established after segmentation is shown in Fig. 5(b). The pore structure of the sandstone is simple. The pore connectivity was good, and the pore and throat volumes were large. The surfaces of the pores and throats were smooth.

A 3D pore network model of sandstone was built based on the maximal ball algorithm (Arand and Hesser, 2017) to calculate the pore characteristic parameters (Hakimov et al., 2022; Edison and Monson, 2012), and the results are shown in Fig. 5(c)–(g). The basic principle of the maximum ball algorithm is to first regularize the irregular pore shape, and then find the maximum inscribed ball radius at any point in the processed pore space (Wang et al., 2023). The pore is represented by the locally largest ball, and the throat is represented by all smaller balls connecting the ball (pore) (Kang et al., 2022). The average pore and throat radii are 48.62 and 31.23 μm, respectively, with an insignificant difference between them. This indicates that the pore structure of the sandstone was relatively homogeneous, with large pores and throats. The coordination number refers to the number of throats connected to a central pore, reflecting the pore connectivity of a core sample. The greater the coordination number, the better the connectivity. The coordination number was 3.21, indicating that the connectivity of sandstone was very good. The tortuosity was 2.92, similar with the results of the sandstone sample calculated by Zhang Y. et al. (2019), indicating that the pore structure of the sandstone was relatively regular. The segmented porosity is 27.40%, slightly lower than 32.14% of N_2 porosity measured with a QKY-II instrument using nitrogen (N_2) as the microporosity below resolution cannot be imaged. The segmented permeability calculated based on lattice Boltzmann method (LBM) (Zhang L. et al., 2019; Jiang et al., 2023; Cai et al., 2022) was the same as that measured for the N_2 permeability, which was 22 D.

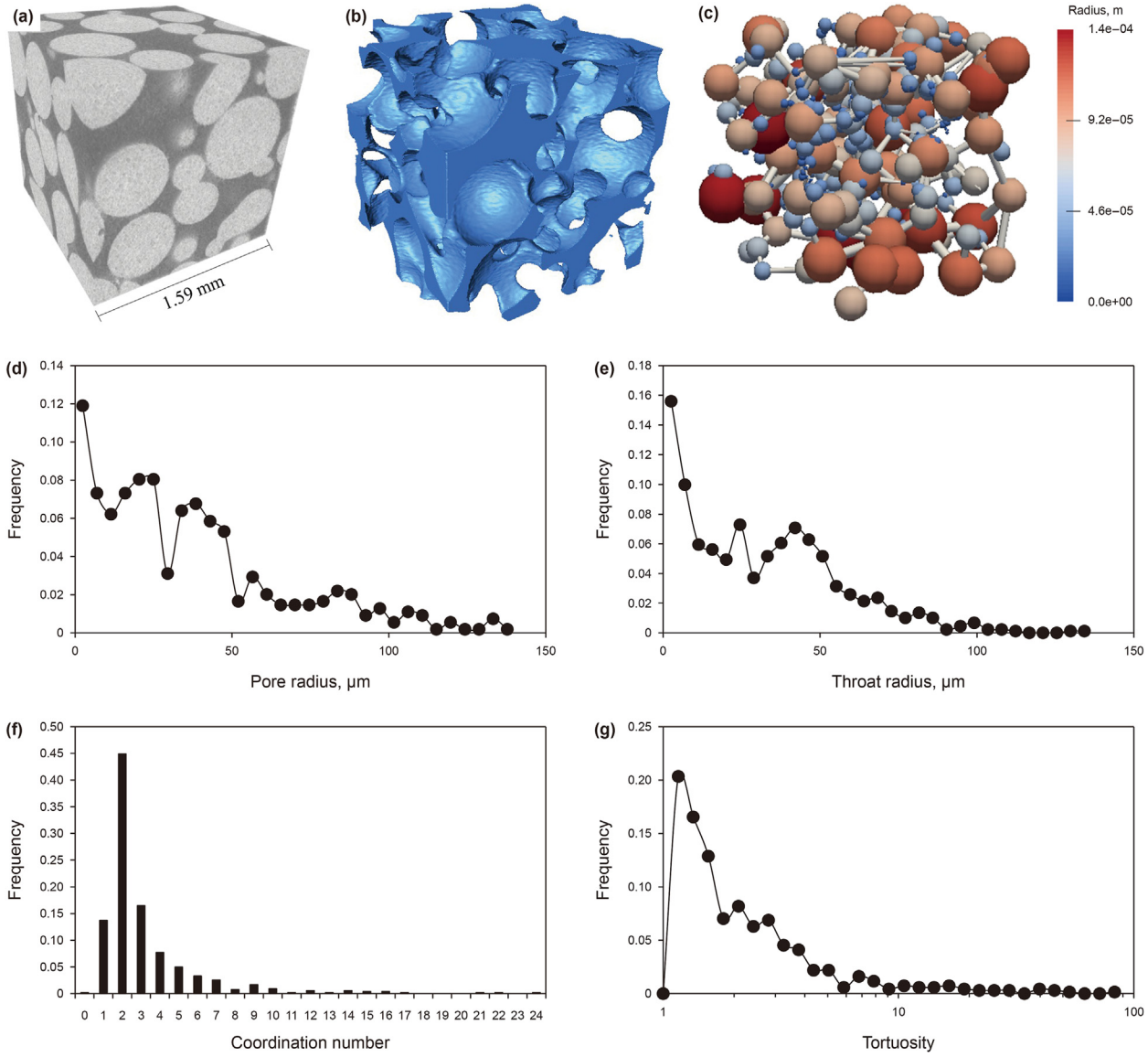

Fig. 5. 3D visualization (400 × 400 × 400 voxel size) and the pore network model of the sandstone sample at 4 μm voxel resolution. (**a**) Sandstone sample; (**b**) Pore space of the sample; (**c**) Pore network model of the sample; Distribution of pore radius (**d**), throat radius (**e**), coordination number (**f**), and tortuosity (**g**).

3.2. Phase behavior of gas condensate in sandstone pores

3.2.1. Phase behavior dynamic evolution

The pressure of the gas condensate system was first increased to 16.0 MPa and the sandstone core was saturated with gas condensate. Then, depressurization was performed to explore the dew point pressure of the gas condensate in the sandstone. 2D slice images of the gas condensate in the porous media under different pressures are shown in Fig. 6. When the pressure decreases from 12.8 to 12.7 MPa, the gray value of sandstone pores in the image appears changed. There is a small amount of dark gray material on the surface of the sandstone pores, which is the condensate liquid. Therefore, the dew point pressure of gas condensate in sandstone is 12.7 MPa, which is 0.7 MPa higher than the dew point pressure of gas condensate in the PVT cell (12.0 MPa). This indicates that porous media can increase the dew point pressure of the gas condensate, owing to the joint influences of adsorption on the pore surface and capillary condensation.

It is known that every medium shows adsorption. However, the adsorption capacity can be strong or weak depending on the pore structure of the core, the volume and shape of the pores and throats, the specific surface area, and the temperature and pressure of the system (Lyman et al., 1992; Tsau et al., 2022; Zhang et al., 2013; Zhong et al., 2017, 2018b; Jatukaran et al., 2018). According to the theory of solid physics, molecules on a solid surface have higher energy than molecules inside the solid (Sattari et al., 2016). The forces between the molecules on the surface are unbalanced or unsaturated (Gao et al., 2019; El-Sheikh et al., 2006). The cores adsorb gas molecules to their surfaces through van der Waals force (Teklu et al., 2014), so that the molecular forces on their surfaces reach equilibrium, and an adsorption layer (also known as an adsorption film whose thickness is generally not considered) is formed (Abolghasemi and Andersen, 2020). The larger the specific surface area, the stronger the adsorption capacity. Because of the weak attractive interaction between the solid surface and gas molecules, the molecular structure and composition of the adsorbate (gas condensate) undergo no change, and the composition of the adsorption layer is the same as that of the adsorbate (Jin and Coasne, 2017). The specific surface areas of the pores are much larger than those of the PVT cells. Therefore, the number and area of the adsorption layers formed by the gas condensate on the surface of the pores were much higher than those of the adsorption layers formed on the surface of the PVT cell. With a decrease in the system pressure, the intermolecular distance in the gas condensate system increased, the intermolecular repulsion decreased, and the intermolecular attractive force dominated. Owing to the large attractive force of heavy hydrocarbon molecules, the heavy hydrocarbon components in the adsorption layer preferentially desorb from the surface and enter the gas phase (Li et al., 2015). This results in a decrease in the content of heavy hydrocarbon components in the adsorption layer and an increase in the relative content of light hydrocarbon components. The heavy hydrocarbon content in the gas condensate system increased, whereas the light hydrocarbon content relatively decreased. In the depressurization process, the increase in the heavy component content of the gas condensate system in the pores was greater than that in the PVT cell. The higher the heavy component content, the higher the dew point pressure of the gas condensate system (Aniefiok, 2015). Therefore, retrograde condensation of the gas condensate in the depressurization process occurred earlier than that in the PVT cell.

Furthermore, when the gas condensate system forms adsorption layers on the surface of the pores, the thickness of the adsorption layers is negligible compared to the pore space and can be generally ignored. However, when adsorption layers are formed in nanopores or nanothroats, the thickness of the adsorption layers cannot be ignored (Yang et al., 2019). These adsorption layers contact and merge with each other, and finally condense to form a meniscus under the influence of capillary force, resulting in capillary condensation (Kikkinides et al., 1999). Thus, the gas condensate system in porous media, including nanopores, underwent retrograde condensation earlier than that in the PVT cell.

The distribution and volume proportion of the condensate liquid and gas condensate in the porous media during pressure depletion are shown in Fig. 7. At the dew point pressure, the condensate liquid condenses into small pores, narrow throats, pore corners, and some surfaces of the pores and throats. With a decrease in pressure, an increasing amount of condensate liquid was formed. It converges from small pores, narrow throats, and pore corners, spreads around the surface, and covers nearly the entire surface of the pores and throats. In the initial stage of depressurization, the amount of condensate liquid increased rapidly. The volume proportion of the condensate liquid increased from 5.94% to 26.41%. The content of the condensate liquid in each pore and throat increased. Until the maximum liquid dropout, P_{max} (10.0 MPa, as shown in Fig. 7), was reached, the condensate liquid existed in almost all pores and throats, and the volume proportion of the condensate liquid reached 30.74%. Subsequently, as the pressure continued to decrease, the condensate liquid molecules began to evaporate into the gas condensate. The amount of condensate liquid decreased, but the rate of decrease was slow due to the influence of adsorption. First, the condensate liquid clusters that were connected or partially connected in the pores were separated. Next, the thickness of the condensate liquid covering the surfaces of the pores and throats gradually decreased. The condensate liquid completely disappeared on some smooth surfaces of the pores with large volumes. The amount of condensate

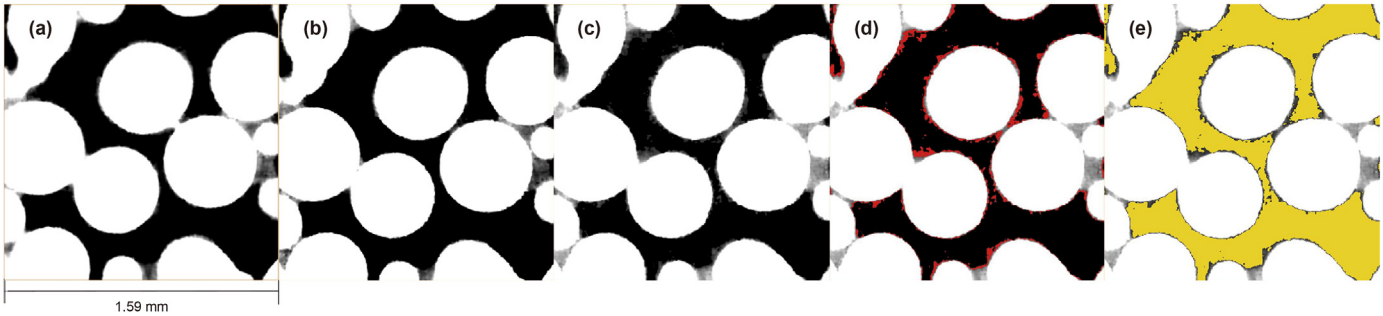

Fig. 6. 2D slice images of the dry sample (**a**) and gas condensate in the porous media at 12.8 MPa (**b**) and 12.7 MPa (**c**), in which *black* area represents gas condensate, *white* area represents skeleton, *light gray* area represents epoxy resin and *dark gray* area around skeleton represents condensate liquid. 2D images of condensate liquid (*colored red*) (**d**) and gas condensate (*colored yellow*) (**e**) in porous media under 12.7 MPa.

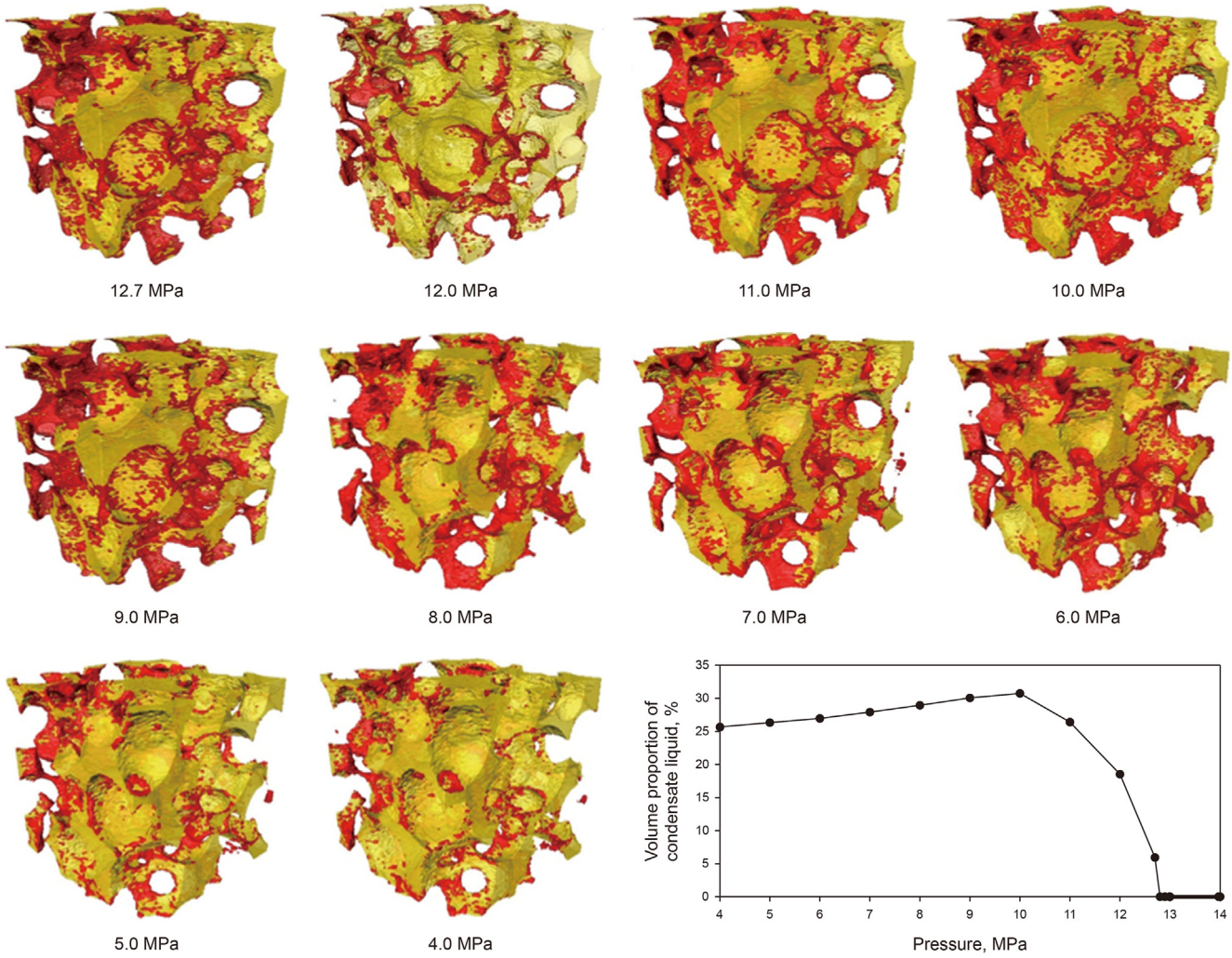

Fig. 7. Distribution and volume proportions of gas condensate (*yellow*) and condensate liquid (*red*) in porous media under different pressures.

liquid in the small pores, narrow throats, and pore corners gradually decreased. After reaching the minimum pressure (4.0 MPa) in the experiment, owing to the inability to reach the lower dew point, some condensate liquid remained in the pores, and the system was in a two-phase gas–liquid state. The volume proportion of the condensate liquid at 4.0 MPa was 25.67%. Generally, the amount of condensate liquid generated from the gas condensate during pressure depletion in porous media first increased and then decreased. The change in the condensate liquid content occurred simultaneously and synchronously throughout the porous media.

3.2.2. Changes of physical properties of condensate liquid

After the condensate liquid and gas condensate in the porous media were separated and extracted from the CT scanning images to establish digital cores and pore network models, some characteristic parameters of the condensate liquid under different pressures were calculated to investigate the physical property changes of the condensate liquid during pressure depletion. The calculation results for the characteristic parameters of the condensate liquid are shown in Fig. 8. An independent condensate liquid is regarded as a separate condensate liquid ganglion. As shown in Fig. 8(a), the average radius of the condensate liquid ganglia first increased and then decreased. When the pressure decreased from the dew point pressure (12.7 MPa) to P_{max} (10.0 MPa), the average radius of the condensate liquid ganglia increased rapidly. When P_{max} was reached, the average radius of condensate liquid ganglia reached a maximum of 8.27 μm. When the pressure was less than P_{max}, the average radius of the condensate liquid ganglia began to decrease; however, the rate of decrease was slow.

The average coordination number and tortuosity of the condensate liquid ganglia determine the connectivity and curvature of the condensate liquid in the porous media. As shown in Fig. 8(b), the average coordination number and tortuosity of the condensate liquid ganglia did not change significantly. The average coordination number of the condensate liquid ganglia increased when the system pressure was between the dew point pressure and P_{max}, and decreased when it was less than P_{max}. This indicates that the content and volume of the condensate liquid increased continuously from the dew point pressure to P_{max}, and some unconnected condensate liquid ganglia gradually converged and merged into a larger connected condensate liquid ganglion. When the pressure was less than P_{max}, the content of the condensate liquid decreased, and a small portion of the condensate liquid ganglia with good connectivity was split into several smaller condensate liquid ganglia with poor connectivity. As shown in Fig. 8(c), the average tortuosity of the condensate liquid ganglia decreased when the system pressure was between the dew point pressure and P_{max} and increased when the system pressure was less

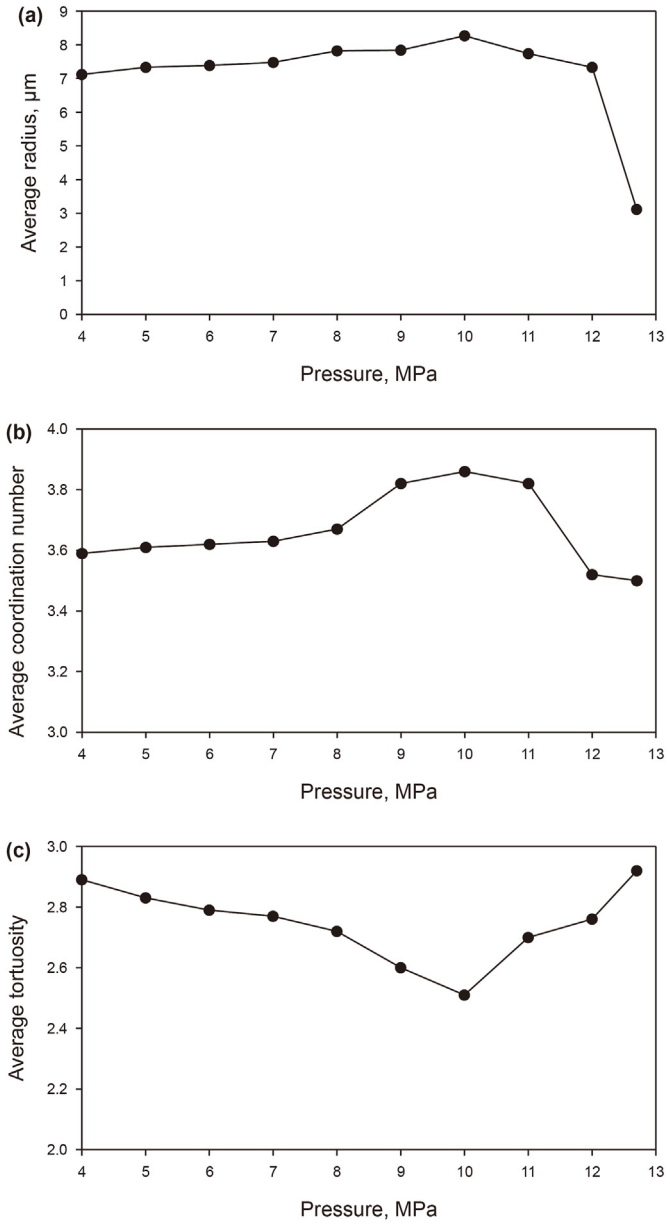

Fig. 8. Characteristic parameters of condensate liquid in porous media under different pressures. (**a**) Average radius; (**b**) Average coordination number; (**c**) Average tortuosity.

than P_{max}. When the system pressure increased from the dew point pressure to P_{max}, owing to the small amount of condensate liquid at the beginning, the thickness of the condensate liquid ganglia stored on the surface and pore corners was small, and their shapes were mainly determined by their locations. The condensate liquid ganglia are initially stored in small pores, throats, and pore corners with complex morphologies leading to high tortuosity. With a decrease in pressure, the content of the condensate liquid increased continuously, and the thickness of the condensate liquid ganglia that originally existed on the surface of small pores and throats gradually increased, making the shape more regular, and the tortuosity continuously reduced. When the system pressure was less than P_{max}, the condensate liquid content gradually decreased. The thickness of the condensate liquid ganglia gradually decreased. Their shape was much closer to the shapes of pores, throats, and pore corners, leading to a continuous increase in the average tortuosity of the condensate liquid ganglia.

3.2.3. Morphology and distribution of condensate liquid

The change in the occurrence state of condensate liquid is one of the manifestations of the phase behavior characteristics of gas condensate. Besides, the remaining condensate liquid in the porous media has been hindering the development of gas condensate reservoirs. During pressure depletion, the condensate liquid has many different occurrence states in porous media. Understanding the occurrence state of condensate liquid in porous media is of great significance for the development of gas condensate reservoirs. The size, morphology, and formation of the condensate liquid in different occurrence states vary, and the condensate liquid must be classified to perform a more targeted analysis. Shape factor, *G*, (Mason and Morrow, 1991; Prodanović et al., 2007) and Euler number, *Eu*, (Kong and Rosenfeld, 1989) are introduced to distinguish the types of condensate liquid under different pressures (Mohamed et al., 2020; Schlüter et al., 2016). Jing et al. (2022) have presented specific definitions of these two parameters.

The classification criteria for the condensate liquid types are listed in Table 2. Condensate liquid ganglia are divided into four types based on their shape factors and Euler number: clustered, branched, membranous, and droplet ganglia (Jing et al., 2022; Li et al., 2017a). Among them, clustered ganglia are the most complex, with the largest volume and the best connectivity. They are distributed in the form of emissions and can simultaneously connect multiple pores and throats at the same time. Branched ganglia are similar in shape to clustered ganglia, but much smaller in volume than clustered ganglia. Generally, they extend in only two or three directions, connecting only a few pores and throats. Membranous ganglia exist on the regular surfaces of pores and throats. Their thicknesses and volumes are small; however, their extension ranges are large. Droplet ganglia exist in small pores and pore corners with regular shape like water droplets. They have the smallest volume compared to the other condensate liquid types.

The volume proportion, number, and average volume of different types of condensate liquid under different pressures are shown in Figs. 9–11. The volume proportion herein is the percentage of the volume of a certain type of condensate liquid in the

Table 2
The classification criteria of condensate liquid.

Type	Classification criteria	Typical figure
Clustered	$G \leq 0.1$, $Eu < 1$	
Droplet	$G \geq 0.9$	
Membranous	$0.1 < G < 0.9$, $Eu \geq 1$	
Branched	The other	

total volume considering all types of condensate liquid and refers to the total quantity of a certain type of condensate liquid. The average volume refers to the ratio of the total volume of a certain type of condensate liquid ganglia to the number of its ganglia. During the process of pressure depletion, the condensate liquid in porous media is mostly in the form of clustered ganglia, whose volume proportion exceeds 98%. The volume proportions of branched, membranous, and droplet ganglia are very small. This is because, due to the good pore connectivity of the sandstone (coordination number is 3.21), condensate liquid first adheres to the surfaces of the pores and throats after precipitation and is interconnected into clusters, forming large clustered ganglia with large average volumes. The average volume of branched, membranous, and droplet ganglia is much smaller than that of clustered ganglia. Although their quantity is greater, their volume proportion is still much smaller than that of clustered ganglia.

At dew point pressure, due to the small overall volume proportion of the condensate liquid (5.94%), except for some clustered ganglia, most condensate liquid ganglia only gathered locally in pores and throats and were not connected. Therefore, the number of all types of condensate liquid ganglia is large, but the average volume is relatively small, as shown in Figs. 10 and 11. Subsequently, with a continuous decrease in pressure, an increasing amount of condensate liquid was generated. The condensate liquid ganglia were gradually interconnected, forming a clustered ganglion with a large volume. The branched ganglia with larger volume, more complex shape, and better connectivity compared to membranous and droplet ganglia, were almost all transformed into a part of the clustered ganglion. Only a small number of branched ganglia with small volumes existed at some small throats with poor connectivity. Therefore, as the pressure decreased after dew point pressure, the number and average volume of branched ganglia decreased. The average volume of membranous and droplet ganglia was very small and the connectivity was poor, and they distributed on the surfaces of the pores and throats of the entire sandstone. As the pressure decreased, they were also partially converted into other types of condensate liquid ganglia, resulting in a decrease in quantity, as shown in Fig. 10. However, due to the poor connectivity of the membranous and droplet ganglia, most of them still existed in independent states. Therefore, with the increase in the entire condensate liquid content, the average volume of the membranous and droplet ganglia also slightly increased, as shown in Fig. 11.

After the maximum liquid dropout, with decreasing pressure, the content of the condensate liquid decreased. The average

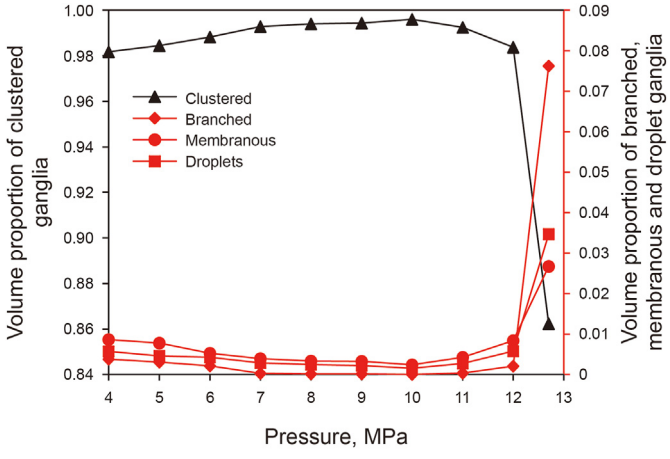

Fig. 9. Volume proportion of different types of condensate liquid in porous media under different pressures.

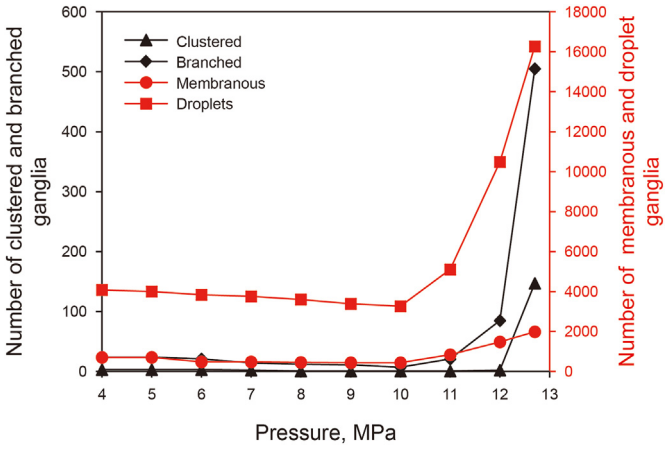

Fig. 10. Number of different types of condensate liquid in porous media under different pressures.

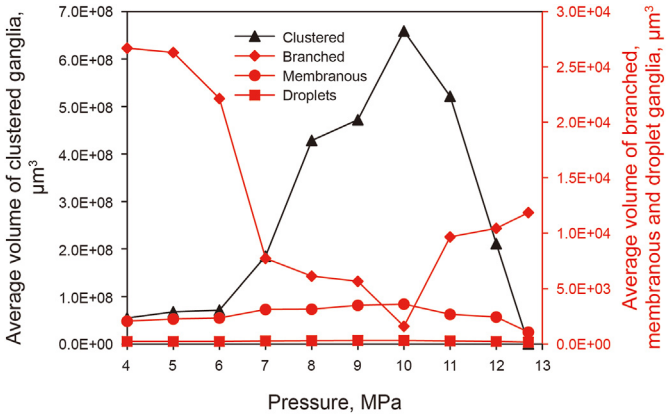

Fig. 11. Average volume of different types of condensate liquid in sandstone pores under different pressures.

volume of clustered, membranous, and droplet ganglia began to decrease. Many condensate liquid ganglia that were originally part of the clustered ganglion were interrupted and separated, forming other types of condensate liquid and smaller clustered ganglia, resulting in a decrease in the volume proportion of the clustered ganglia and a slight increase in the number. The volume proportion of the other three types of condensate liquid was slightly increased. Among them, the volume of the branched ganglia formed by the disconnection of the clustered ganglia was relatively large, so the average volume and number of the branched ganglia increased. The volume of newly formed membranous and droplet ganglia was very small, so the number of them slightly increased but the average volume slightly decreased, as shown in Figs. 10 and 11.

4. Conclusions

The remaining condensate liquid caused by the phase transition that occurs in actual porous media in the process of gas condensate depletion production greatly reduces the recovery. It is significant to figure out the phase behavior dynamically changing process of gas condensate in porous media during pressure depletion. In this study, a gas condensate pressure depletion experiment was conducted using real-time CT scanning to investigate the phase behavior of gas condensate in porous media. The phase behavior changing process and mechanism of gas condensate in the PVT cells

and porous media were proven to be different. The morphology, state of occurrence, and characteristics of the condensate liquid during the pressure depletion process were dynamically observed and analyzed. Summarizing the results of this investigation, the main conclusions are as follows.

(1) Porous media influence the phase behavior of gas condensate. Specifically, the dew point pressure of gas condensate in porous media is 12.7 MPa, which is 0.7 MPa higher than that of gas condensate in a PVT cell at 12.0 MPa. The retrograde condensation phenomenon, caused by adsorption and capillary condensation, is advanced.
(2) When the phase behavior of gas condensate changes in porous media, the condensate liquid is generated in pores with small radius, narrow throats, and pore corners. The amount of condensate liquid in the porous media first increases and then decreases during pressure depletion. The changes in the condensate liquid content occur simultaneously and synchronously throughout the porous media.
(3) From the calculation results of the characteristic parameters of condensate liquid based on the pore network model, the average radius and volume of the condensate liquid ganglia increase rapidly after reaching the dew point pressure. Below the maximum liquid dropout, P_{max} (10.0 MPa), the radius and volume of the condensate liquid ganglia decrease; however, the rate of decrease is slow. This is because with a decrease in pressure, the distance between molecules increases, and attractive forces play a major role. It is difficult to separate liquid hydrocarbons from condensate liquid because of their high molecular weights and strong intermolecular attractive forces. The connectivity of the condensate liquid ganglia increases from the dew point pressure to P_{max} and then decreases after P_{max}. The tortuosity of the condensate liquid ganglia decreases from the dew point pressure to P_{max} and increases below P_{max}.
(4) According to the shape factor and Euler number, condensate liquid can be classified into four types: clustered, branched, membranous, and droplet ganglia. During pressure depletion, the condensate liquid is mainly distributed in the form of clustered ganglia, followed by branched and membranous ganglia, and the volume proportion of droplet ganglia is the lowest.

CRediT authorship contribution statement

Wen-Long Jing: Conceptualization, Data curation, Formal analysis, Investigation, Methodology, Software, Validation, Visualization, Writing – original draft, Writing – review & editing. **Lei Zhang:** Conceptualization, Funding acquisition, Investigation, Methodology, Project administration, Resources, Supervision, Writing – review & editing. **Ai-Fen Li:** Conceptualization, Formal analysis, Methodology, Project administration, Resources, Supervision, Writing – review & editing. **Jun-Jie Zhong:** Formal analysis, Funding acquisition, Investigation, Methodology, Resources, Supervision. **Hai Sun:** Funding acquisition, Investigation, Resources, Supervision. **Yong-Fei Yang:** Investigation, Methodology, Software. **Yu-Long Cheng:** Data curation, Investigation, Validation, Visualization. **Jun Yao:** Conceptualization, Investigation, Methodology, Project administration, Resources.

Declaration of competing interest

The authors declare that they have no financial and personal relationships with other people or organizations that can inappropriately influence our work. There is no professional or other personal interest of any nature or kind in any product, service and/or company that could be construed as influencing the position presented in, or the review of, the manuscript entitled.

Acknowledgements

We would like to express appreciation to the following financial support: the National Natural Science Foundation of China (Nos. 52122402, 12172334, 52034010, 52174051), Shandong Provincial Natural Science Foundation (Nos. ZR2021ME029, ZR2022JQ23), and Fundamental Research Funds for the Central Universities (No. 22CX01001A-4).

References

Abolghasemi, E., Andersen, P., 2020. Influence of adsorption layer thickness and pore geometry in tight compressible shales subject to gas production. In: SPE Asia Pacific Oil & Gas Conference and Exhibition. https://doi.org/10.2118/202309-MS.
Ahmed, T., 2016. Equations of State and PVT Analysis: Applications for Improved Reservoir Modeling. Gulf Professional Publishing, pp. 1–69. https://doi.org/10.1016/C2014-0-00119-0.
Aniefiok, L., 2015. Ranking of C_{6+} composition split schemes of pipeline gas for hydrocarbon dewpoint determination. In: SPE Nigeria Annual International Conference and Exhibition. https://doi.org/10.2118/178372-MS.
Arabloo, M., Shokrollahi, A., Gharagheizi, F., et al., 2013. Toward a predictive model for estimating dew point pressure in gas condensate systems. Fuel Process. Technol. 116, 317–324. https://doi.org/10.1016/j.fuproc.2013.07.005.
Arand, F., Hesser, J., 2017. Accurate and efficient maximal ball algorithm for pore network extraction. Comput. Geosci. 101, 28–37. https://doi.org/10.1016/j.cageo.2017.01.004.
Barnes, R., Lehman, C., Mulla, D., 2014. Priority-flood: an optimal depression-filling and watershed-labeling algorithm for digital elevation models. Comput. Geosci. 62, 117–127. https://doi.org/10.1016/j.cageo.2013.04.0.
Buades, A., Coll, B., Morel, J.M., 2005. A non-local algorithm for image denoising. In: IEEE Computer Conference on Computer Vision and Pattern Recognition (CVPR'05). https://doi.org/10.1109/CVPR.2005.38.
Cai, J., Chen, Y., Qiao, J., et al., 2022. Determination of dynamic capillary effect on two-phase flow in porous media: a perspective from various methods. Petrol. Sci. 19 (4), 1641–1652. https://doi.org/10.1016/j.petsci.2022.01.017.
Cousty, J., Bertrand, G., Najman, L., et al., 2009. Watershed cuts: minimum spanning forests and the Drop of water Principle. IEEE Trans. Pattern Anal. Mach. Intell. 31 (8), 1362–1374. https://doi.org/10.1109/TPAMI.2008.173.
Dodson, C.R., Goodwill, D., Mayer, E.H., 1953. Application of laboratory PVT data to reservoir engineering problems. J. Petrol. Technol. 5 (12), 287–298. https://doi.org/10.2118/953287-G.
Edison, J.R., Monson, P.A., 2012. Dynamic mean field theory of condensation and evaporation in model pore networks with variations in pore size. Microporous Mesoporous Mater. 154 (15), 7–15. https://doi.org/10.1016/j.micromeso.2011.12.029.
El-Sheikh, S.M., Barakat, K., Salem, N.M., 2006. Phase transitions of methane using molecular dynamics simulations. J. Chem. Phys. 124, 124517. https://doi.org/10.1063/1.2179422.
Fang, H., Wang, Z., Sang, S., et al., 2023. Numerical analysis of matrix swelling and its effect on microstructure of digital coal and its associated permeability during CO_2-ECBM process based on X-ray CT data. Petrol. Sci. 20 (1), 87–101. https://doi.org/10.1016/j.petsci.2022.07.011.
Faraji, F., Ugwu, J.O., Nabhani, F., et al., 2019. Development of inflow performance model in high temperature gas-condensate reservoirs. J. Petrol. Sci. Eng. 181, 106169. https://doi.org/10.1016/j.petrol.2019.06.033.
Gao, Y., Wu, K., Yang, S., et al., 2019. The effect of surface-gas interaction on mean free path for gases confined in nanopores of shale gas reservoirs. In: SPE/AAPG/SEG Unconventional Resources Technology Conference. https://doi.org/10.15530/urtec-2019-284.
Ghiasi, M.M., Shahdi, A., Brati, P., et al., 2014. Robust modeling approach for estimation of compressibility factor in retrograde gas condensate systems. Ind. Eng. Chem. Res. 32, 12872–12887. https://doi.org/10.1021/ie404269b.
Gouda, A., Gomaa, S., Attia, A., et al., 2022. Development of an artificial neural network model for predicting the dew point pressure of retrograde gas condensate. J. Petrol. Sci. Eng. 208. Part E. https://doi.org/10.1016/j.petrol.2021.109284.
Guo, P., Sun, L., Li, S., et al., 1996. A theoretical study of the effect of porous media on the dew point pressure of a gas condensate. In: SPE Gas Technology Symposium. https://doi.org/10.2118/35644-MS.
Hakimov, N., Syed, F., Muther, T., et al., 2022. Pore-scale network modeling approach to study the impact of microporosity's pore space topology. Microporous Mesoporous Mater. 338, 111918. https://doi.org/10.1016/j.micromeso.2022.111918.
Hemes, S., Desbois, G., Urai, J.L., et al., 2015. Multi-scale characterization of porosity

in boom clay (HADES-level, Mol, Belgium) using a combination of X-ray μ-CT, 2D BIB-SEM and FIB-SEM tomography. Microporous Mesoporous Mater. 208 (15), 1–20. https://doi.org/10.1016/j.micromeso.2015.01.022.
Hong, C., Yang, R., Huang, Z., et al., 2023. Enhance liquid nitrogen fracturing performance on hot dry rock by cyclic injection. Petrol. Sci. 20 (2), 951–972. https://doi.org/10.1016/j.petsci.2022.07.004.
Jatukaran, A., Zhong, J., Persad, A.H., et al., 2018. Direct visualization of evaporation in a two-dimensional nanoporous model for unconventional natural gas. ACS Appl. Nano Mater. 1 (3), 1332–1338. https://doi.org/10.1021/acsanm.8b00064.
Jiang, C., Zhou, H., Xia, M., et al., 2023. A joint absorbing boundary for the multiple-relaxation-time lattice Boltzmann method in seismic acoustic wavefield modeling. Petrol. Sci. 20 (4), 2113–2126. https://doi.org/10.1016/j.petsci.2023.02.019.
Jin, D., Coasne, B., 2017. Molecular simulation of the phase diagram of methane hydrate: free energy calculations, direct coexistence method, and hyperparallel tempering. Langmuir 33 (42), 11217–11230. https://doi.org/10.1021/acs.langmuir.7b02238.
Jing, W., Zhang, L., Li, A., et al., 2022. Investigation of pore-scale remaining oil dynamic evolution in heterogeneous marine carbonate using real-time CT scanning. Energy & Fuels 36 (15), 8180–8188. https://doi.org/10.1021/acs.energyfuels.2c01497.
Kang, J., Li, N., Zhao, L., et al., 2022. Construction of complex digital rock physics based on full convolution network. Petrol. Sci. 19 (2), 651–662. https://doi.org/10.1016/j.petsci.2021.11.018.
Kikkinides, E.S., Stubos, A.K., Tzevelekos, K.P., et al., 1999. Ceramic membranes - characterization and applications. Stud. Surf. Sci. Catal. 120 (Part A), 687–713. https://doi.org/10.1016/S0167-2991(99)80569-2.
Kong, T.Y., Rosenfeld, A., 1989. Digital topology: introduction and survey. Comput. Vis. Graph Image Process 48 (3), 357–393. https://doi.org/10.1016/0734-189X(89)90147-3.
Li, J., Yu, B., 2022. Gas properties, fundamental equations of state and phase relationships. Sustainable Natural Gas Reservoir and Production Engineering 1, 1–28. https://doi.org/10.1016/B978-0-12-824495-1.00004-8.
Li, J., Li, X., Shi, J., et al., 2015. Mechanism of liquid-phase adsorption and desorption in coalbed methane systems - a new insight into an old problem. In: SPE Asia Pacific Unconventional Resources Conference and Exhibition. https://doi.org/10.2118/177001-MS.
Li, J., Jiang, H., Wang, C., et al., 2017a. Pore-scale investigation of microscopic remaining oil variation characteristics in water-wet sandstone using CT scanning. J. Nat. Gas Sci. Eng. 48, 36–45. https://doi.org/10.1016/j.jngse.2017.04.003.
Li, J., Zhao, G., Jia, X., et al., 2017b. Integrated study of gas condensate reservoir characterization through pressure transient analysis. J. Nat. Gas Sci. Eng. 46, 104464. https://doi.org/10.1016/j.jngse.2017.07.017.
Li, M., Zhou, F., Liu, J., et al., 2022a. Quantitative investigation of multi-fracture morphology during TPDF through true tri-axial fracturing experiments and CT scanning. Petrol. Sci. 19 (4), 1700–1717. https://doi.org/10.1016/j.petsci.2022.03.017.
Li, Q., Li, X., Zan, K., et al., 2013. Experimental research of critical condensate saturation and flow characteristics of gas condensate reservoir. Petrol. Sci. Technol. 31 (13), 10–18. https://doi.org/10.1080/10916466.2010.543727.
Li, Y., Yang, Y., Dong, M., et al., 2022b. In-situ imaging of CO_2 trapping and oil recovery in three-phase systems: dependence on pore geometry and wettability. SPE J. 28 (2), 768–782. https://doi.org/10.2118/212830-PA.
Luo, S., Chen, F., Zhou, D., et al., 2021. Multiscale pressure/volume/temperature simulation of decreasing condensate/gas ratio at greater than dewpoint pressure in shale gas-condensate reservoirs. SPE J. 26 (6), 4174–4186. https://doi.org/10.2118/203905-PA.
Lyman, W.J., Reehl, W.F., Rosenblatt, D.H., 1992. Handbook of chemical property estimation methods. Molecular Nutrition 36 (2), 218–219. https://doi.org/10.1201/9781420026283.
Mansour, E.M., Aily, M.E., Desouky, S.E.M., 2020. Gases reservoirs fluid phase behavior. Oil and Gas Wells. IntechOpen. https://doi.org/10.5772/intechopen.85610.
Masihi, M., Shams, R., King, P.R., 2022. Pore level characterization of micro-CT images using percolation theory. J. Petrol. Sci. Eng. 211, 110113. https://doi.org/10.1016/j.petrol.2022.110113.
Mason, G., Morrow, N.R., 1991. Capillary behavior of a perfectly wetting liquid in irregular triangular tubes. J. Colloid Interface Sci. 141 (1), 262–274. https://doi.org/10.1016/0021-9797(91)90321-X.
Meyer, F., 1994. Topographic distance and watershed lines. Signal Process. 38 (1), 113–125. https://doi.org/10.1016/0165-1684(94)90060-4.
Mohamed, A.I.A., Khishvand, M., Piri, M., 2020. A pore-scale experimental investigation of process-dependent capillary desaturation. Adv. Water Resour. 144, 103702. https://doi.org/10.1016/j.advwatres.2020.103702.
Moses, P.L., 1986. Engineering applications of phase behavior of crude oil and condensate systems. J. Petrol. Technol. 38 (7), 715–723. https://doi.org/10.2118/15835-PA.
Nguyen, P., Mohaddes, D., Riordon, J., et al., 2015. Fast fluorescence-based microfluidic method for measuring minimum miscibility pressure of CO_2 in crude oils. Anal. Chem. 87 (6), 3160–3164. https://doi.org/10.1021/ac5047856.
Noor, I., Martin, A., Dahl, O., 2020. Water recovery from flue gas condensate in municipal solid waste fired cogeneration plants using membrane distillation. Chem. Eng. J. 399 (1), 125707. https://doi.org/10.1016/j.cej.2020.125707.
Potsch, K., Toplack, P., Gumpenberger, T., 2017. A review and extension of existing consistency tests for PVT data from a laboratory. SPE Reservoir Eval. Eng. 20 (2), 269–284. https://doi.org/10.2118/183640-PA.
Prodanović, M., Lindquist, W.B., Seright, R.S., 2007. 3D image-based characterization of fluid displacement in a Berea core. Adv. Water Resour. 30, 214–226. https://doi.org/10.1016/j.advwatres.2005.05.015.
Qi, Z., Liang, B., Deng, R., et al., 2007. Phase behavior study in the deep gas-condensate reservoir with low permeability. In: EUROPEC/EAGE Conference and Exhibition. https://doi.org/10.2118/107315-MS.
Raghavan, R., Jones, J., 1996. Depletion performance of gas-condensate reservoirs. J. Petrol. Technol. 48 (8), 725–731. https://doi.org/10.2118/36352-JPT.
Reis, P.K.P., Carvalho, M.S., 2022. Pore-scale analysis of gas injection in gas-condensate reservoirs. J. Petrol. Sci. Eng. 212, 110189. https://doi.org/10.1016/j.petrol.2022.110189.
Sattari, M., Abedi, J., Zirrahi, M., et al., 2016. Modeling the onset of asphaltene precipitation in solvent-diluted bitumens using cubic-plus-association equation of state. In: SPE Canada Heavy Oil Technical Conference. https://doi.org/10.2118/180725-MS.
Saarinen, K., 1994. Color image segmentation by a watershed algorithm and region adjacency graph processing. In: 1st International Conference on Image Processing. https://doi.org/10.1109/ICIP.1994.413690.
Saeidi, A., Handy, L.L., 1974. Flow and phase behavior of gas condensate and volatile oils in porous media. In: SPE California Regional Meeting. https://doi.org/10.2118/4891-MS.
Scanziani, A., Alhammadi, A., Bijeljic, B., et al., 2018. Three-phase flow visualization and characterization for a mixed-wet carbonate rock. In: Abu Dhabi International Petroleum Exhibition & Conference. https://doi.org/10.2118/192666-MS.
Schlüter, S., Berg, S., Rücker, M., et al., 2016. Pore-scale displacement mechanisms as a source of hysteresis for two-phase flow in porous media. Water Resour. Res. 52, 2194–2205. https://doi.org/10.1002/2015WR018254.
Shapiro, A.A., Stenby, E.H., 1999. High pressure multicomponent adsorption in porous media. Fluid Phase Equil. 158–160, 565–573. https://doi.org/10.1016/S0378-3812(99)00144-2.
Shapiro, A.A., Potsch, K., Kristensen, J.G., et al., 2000. Effect of low permeable porous media on behavior of gas condensates. In: SPE European Petroleum Conference. https://doi.org/10.2118/65182-MS.
Sigmund, P., Dranchuk, P., Morrow, N., et al., 1973. Retrograde condensation in porous media. SPE J. 13 (2), 93–104. https://doi.org/10.2118/3476-PA.
Sui, S., Guo, P., Du, J., et al., 2010. Experimental study on gas condensate depletion in low permeability porous media. Journal of Southwest Petroleum University (Science & Technology Edition) 32 (3), 97–100. https://doi.org/10.3863/j.issn.1674-5086.2010.03.018 (in Chinese).
Sun, Y., Zhan, Y., Yuan, L., 2018. Quantifying nano-pore heterogeneity and anisotropy in gas shale by synchrotron radiation nano-CT. Microporous Mesoporous Mater. 258 (1), 1–20. https://doi.org/10.1016/j.micromeso.2017.08.049.
Teklu, T.W., Alharthy, N., Kazemi, H., et al., 2014. Phase behavior and minimum miscibility pressure in nanopores. SPE Reservoir Eval. Eng. 17 (3), 396–403. https://doi.org/10.2118/168865-PA. SPE-168865-PA.
Tong, M., Li, X., Hu, Y., et al., 2004. Experimental study on influence of porous media on phase behavior of gas condensate. Journal of the University of Petroleum China 28 (5), 61–64. https://doi.org/10.3321/j.issn:1000-5870.2004.05.013.
Tsau, J., Barati, R.G., Zaghloul, J., et al., 2022. Experimental investigation of high pressure, high temperature (HPHT) adsorption of methane and natural gas on shale gas samples. In: ADIPEC. https://doi.org/10.2118/210981-MS.
Tu, H., Zhou, M., Gu, Y., et al., 2022. Preparation and characterization of super hydrophobic/oleophobic material and its application in releasing liquid locking in tight gas condensate reservoirs. J. Petrol. Sci. Eng. 212, 110281. https://doi.org/10.1016/j.petrol.2022.110281.
Wang, C., Yang, Y., Han, D., et al., 2023. Influence of matrix physical properties on flow characteristics in dual network model. Petrol. Sci. 20 (4), 2244–2252. https://doi.org/10.1016/j.petsci.2023.06.006.
Wang, C., Zeng, J., Zhang, G., et al., 2022. Formation processes of gas condensate reservoirs in the Baiyun depression: insights from geochemical analyses and basin modeling. J. Nat. Gas Sci. Eng. 100, 104464. https://doi.org/10.1016/j.jngse.2022.104464.
WcCain, W.D., 2002. Analysis of black oil PVT reports revisited. In: SPE Annual Technical Conference and Exhibition. https://doi.org/10.2118/77386-MS.
Weinaug, C., Cordell, J., 1949. Revaporization of butane and pentane from sand. Transactions of the AIME 179 (1), 303–312. https://doi.org/10.2118/949303-G.
Will, R., Sun, Q., Ayala, L.F., 2018. A compositional rescaled exponential model for multiphase-production-performance analysis of boundary-dominated gas/condensate reservoirs. SPE J. 24 (2), 618–646. https://doi.org/10.2118/192178-PA.
Wu, Y., Wang, D., Wei, J., et al., 2022. Damage constitutive model of gas-bearing coal using industrial CT scanning technology. J. Nat. Gas Sci. Eng. 101, 104543. https://doi.org/10.1016/j.jngse.2022.104543.
Yang, G., Chai, D., Fan, Z., et al., 2019. Analytical investigation of the confinement effect on capillary condensation pressure of fluids in nanopores. In: SPE Western Regional Meeting. https://doi.org/10.2118/195273-MS.
Zhang, A., Fan, Z., Zhao, L., 2020. An investigation on phase behaviors and displacement mechanisms of gas injection in gas condensate reservoir. Fuel 268 (15), 117373. https://doi.org/10.1016/j.fuel.2020.117373.
Zhang, L., Jing, W., Yang, Y., et al., 2019a. The investigation of permeability calculation using digital core simulation technology. Energies 12 (17), 3273. https://doi.org/10.3390/en12173273.
Zhang, T., Murphy, M., Yu, H., et al., 2013. Investigation of nanoparticle adsorption during transport in porous media. In: SPE Annual Technical Conference and

Exhibition. https://doi.org/10.2118/166346-MS.
Zhang, Y., Moghanloo, R.G., Davudov, D., 2019b. Pore structure characterization of a shale sample using SEM images. In: SPE Western Regional Meeting. https://doi.org/10.2118/195352-MS.
Zhong, J., Zandavi, S.H., Li, H., et al., 2017. Condensation in one-dimensional dead-end namochannels. ACS Nano 11 (1), 304–313. https://doi.org/10.1021/acsnano.6b05666.
Zhong, J., Riordon, J., Zandavi, S.H., et al., 2018a. Capillary condensation in 8 nm deep channels. J. Phys. Chem. Lett. 9 (3), 497–503. https://doi.org/10.1021/acs.jpclett.7b03003.
Zhong, J., Zhao, Y., Lu, C., et al., 2018b. Nanoscale phase measurement for the shale challenge: multicomponent fluids in multiscale volumes. Langmuir 34, 9927–9935. https://doi.org/10.1021/acs.langmuir.8b01819.
Zhu, W., Huang, K., Sun, Y., et al., 2020. Theoretical study on the injected gas override in gas condensate reservoirs. Fuel 266 (15), 116977. https://doi.org/10.1016/j.fuel.2019.116977.